

# Finite-Core Vortex Array Model of the Wake of a Periodically Pitching Airfoil

A. M. Naguib,\* J. Vitek,<sup>†</sup> and M. M. Koochesfahani<sup>‡</sup>

*Michigan State University, East Lansing, Michigan 48824*

DOI: 10.2514/1.J050881

In this study, a simple vortex array model is employed to compute the unsteady velocity field in the wake of an airfoil undergoing harmonic as well as nonharmonic pitch oscillation. The parameters of the model are determined by minimizing the difference between the model predictions and existing single-component laser Doppler velocimetry measurements of the streamwise velocity in the near wake of an oscillating NACA 0012 airfoil, at a chord Reynolds number of 11,400. It is shown that the vortex array model is an effective tool for determination of the wake vortex parameters (circulation, core diameter, spacing, etc.) from pointwise measurements of only the streamwise component of the velocity. This is demonstrated through comparison of the vortex parameters estimated using the model with those obtained directly from whole-field measurements in a similar flow. In addition, the mean streamwise force acting on the airfoil is calculated using the model in conjunction with the integral momentum equation. Comparison of the model-predicted force coefficient and its dependence on the reduced frequency are found to be consistent with published experimental and computational data.

## I. Introduction

RECENTLY there has been great interest in studying the aerodynamics of micro air vehicles (MAVs) because of their potential wide ranging use in defense, environmental-monitoring and homeland security applications. For a typical MAV [1], the small size of the device (wing chord of order of a few centimeters) and relatively slow flying speed (of order 10 m/s) result in a wing chord Reynolds number  $Re_c$  of order  $10^4$ . Understanding of the aerodynamics at this low range of Reynolds numbers is lacking as traditional aerodynamics knowledge is based on high Reynolds number airfoils with thin attached boundary layers that operate under steady or quasi-steady conditions. Faced by the challenges of adequate lift generation in low Reynolds number flight based on traditional aerodynamics, and observation of nature's flying animals, a major departure in MAV aerodynamics is the consideration of flapping wing designs where highly unsteady operating conditions are to be exploited instead of avoided [2–6]. The behavior of flow around airfoils executing highly unsteady motions has of course been studied for decades, starting with the classical unsteady aerodynamic theory of oscillating airfoils [7,8]. Nevertheless, recent studies in MAV aerodynamics have lead to the conclusion that the current state of knowledge, predictive capabilities, and experimental data are insufficient regarding the fundamental unsteady aerodynamics of low Reynolds number MAVs [9].

The objective of the present study is to evaluate the effectiveness of a simplified, vortex array model in computing the time-dependent velocity in the wake of an airfoil undergoing small-amplitude but high-reduced-frequency pitch oscillations at low Reynolds number. As will be demonstrated in this paper, a particularly useful feature of this model is that it can be used in conjunction with measurements of

only single-component of the velocity to identify the characteristics of the wake vortices (circulation, size, spacing, etc.). Another, albeit more challenging, potential application of the model is as a predictive/design tool for the estimation of the mean drag (or thrust) and lift acting on airfoils undergoing pitch, plunge, and/or other types of motion trajectories<sup>§</sup>.

The present investigation is an extension of an earlier study by Koochesfahani [10] of the wake of a NACA 0012 airfoil that is pitching harmonically around the one-quarter-chord point between the angle of attack extremes of  $\pm 2$  and  $\pm 4^\circ$ . In the earlier study, the vortex pattern in the wake of the airfoil and how it depends on the frequency of oscillation was examined using flow visualization. The investigation also employed laser Doppler velocimetry (LDV) measurements of the streamwise velocity, which were coupled with the integral momentum equation to compute the mean streamwise force acting on the airfoil. Koochesfahani [10] found that the force changed from drag to thrust with increasing oscillation frequency, and he was able to correlate this switch with the observed vortex pattern in the wake. However, the identified vortex characteristics relied on the use of flow visualization, which could lead to misinterpretation (see Cimbala et al. [11]). Additionally, no results were reported regarding the wake velocity profiles as function of the oscillation cycle phase.

In the present work, the LDV measurements of Koochesfahani [10] are further analyzed to obtain the phase-averaged streamwise velocity profiles for the case with  $2^\circ$  oscillation amplitude. The results are used to determine the parameters of the vortex array model and identify the characteristics of the wake vortices. Subsequently, the model is employed to reconstruct the unsteady streamwise and transverse velocity in the wake of the airfoil to compute the mean streamwise force acting on the airfoil at different frequencies of oscillation. The vortex characteristics obtained from the model as well as the computed force are compared with counterpart results reported by Bohl [12] and Bohl and Koochesfahani [13] using whole-field molecular tagging velocimetry (MTV) measurements.

## II. Experiment

The experimental data have been reported elsewhere (Koochesfahani [10]). Essential details are briefly described here for completeness. All measurements are conducted in a low-speed water

Presented as Paper 2009-393-641 at the 47th AIAA Aerospace Sciences Meeting including The New Horizons Forum and Aerospace Exposition, Orlando, FL, 5–8 January 2009; received 18 September 2010; revision received 16 December 2010; accepted for publication 27 December 2010. Copyright © 2011 by A. M. Naguib, J. Vitek, and M. M. Koochesfahani. Published by the American Institute of Aeronautics and Astronautics, Inc., with permission. Copies of this paper may be made for personal or internal use, on condition that the copier pay the \$10.00 per-copy fee to the Copyright Clearance Center, Inc., 222 Rosewood Drive, Danvers, MA 01923; include the code 0001-1452/11 and \$10.00 in correspondence with the CCC.

\*Associate Professor, Department of Mechanical Engineering. Senior Member AIAA.

<sup>†</sup>Undergraduate Student, Department of Mechanical Engineering.

<sup>‡</sup>Professor, Department of Mechanical Engineering. Associate Fellow AIAA.

<sup>§</sup>Assuming knowledge of the vortex pattern and strength: a point that requires a separate investigation to relate the wake vorticity flux to a given airfoil's motion trajectory.

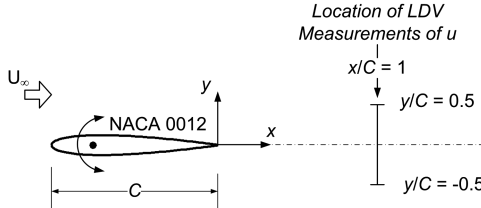


Fig. 1 Sketch of the experimental configuration. The origin of the shown coordinate system does not move with the airfoil (i.e., it is fixed at the trailing edge at  $\alpha = 0$ ).

tunnel. A NACA 0012 wing section with a chord  $C = 8$  cm and a span of 39 cm is pitched about the one-quarter-chord point. Measurement of the streamwise velocity  $u$  is accomplished using LDV in the dual scatter mode at a streamwise location  $x/C = 1$  (see Fig. 1 for a sketch of the experimental configuration and definition of the coordinate system). In the transverse direction, the measurements are conducted at different locations (one location at a time) by traversing the LDV probe volume over the range  $-0.5 < y/C < 0.5$ , which is sufficiently wide to reach into the freestream on either side of the wake. The instantaneous angle of attack of the airfoil  $\alpha$  is recorded simultaneously with the velocity to enable calculation of phase-averaged quantities. The length of the recorded time series is approximately 30 s with successive data points separated by an interval of 15 ms (corresponding to a sampling rate of 66.67 samples/s). Each LDV data point represents an average over this interval.

The freestream velocity  $U_\infty$  is 14.24 cm/s, resulting in a chord Reynolds number of  $Re_c \approx 11,400$ . At this flow condition, the airfoil is pitched harmonically with amplitude  $\alpha_o$  of 2 deg around a mean angle of attack of zero for three oscillation frequencies:  $f = 4$ , 5 and 6 Hz. The corresponding values of the reduced frequency  $k = 2\pi f C / (2U_\infty)$  are 7.1, 8.8, and 10.6. These values are so high such that the mean-velocity profile downstream of the airfoil exhibits no deficit relative to the freestream velocity, or even becomes similar to the profile of a jet rather than a wake flow (see below for further details).

In addition to pure-harmonic oscillation, also examined is a case in which the pitch-up time (i.e., in direction of increasing  $\alpha$ ) is shorter than the pitch-down time at  $f = 4$  Hz ( $k = 7.1$ ). The time-history of  $\alpha$  over one oscillation period for this case is depicted in Fig. 2 in comparison to that of harmonic oscillation. The distinction between the two cases is characterized by a symmetry parameter  $S$ , which is defined as the pitch-up duration  $T_{pu}$  (see Fig. 2 for definition) divided by the oscillation period  $T$ . For the nonharmonic oscillation profile shown in Fig. 2,  $S = 38\%$  (in contrast to  $S = 50\%$  for the harmonic case).

### III. Vortex Array Model

Employing the flow visualization images displayed in Fig. 3, Koochesfahani [10] showed that in all pure-harmonic-oscillation cases, the wake of the airfoil is dominated by the shedding of a

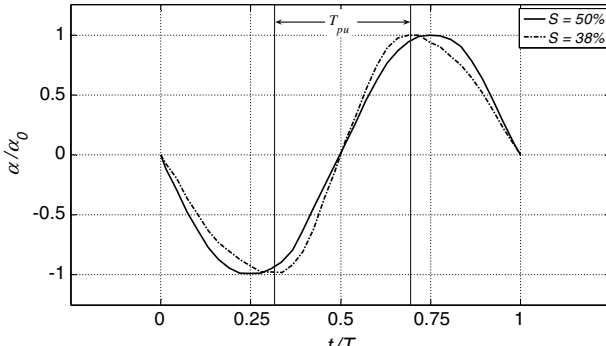


Fig. 2 Time history of the angle of attack for harmonic and nonharmonic oscillation.

counter-rotating pair of vortices per oscillation cycle resulting from the roll up of the boundary-layer vorticity on each side of the airfoil. The key effect of varying the reduced frequency is to alter the relative position of the opposite-sign vortices in the transverse direction. At  $k$  values below 7.1 (not reported here), the vortex locations are qualitatively similar to those of the natural wake in the sense that vortices with positive circulation (i.e., in the counter clockwise direction) are found below the center of the wake and vice versa. The induced velocity of such vortex configuration produces a mean-momentum deficit in the wake. At  $k = 7.1$ , the vortex centers are aligned on the wake's centerline, and a uniform mean-velocity profile with magnitude equal to that of the freestream is established across the entire wake. At higher  $k$  values, the transverse arrangement of the vortex centers becomes opposite to that of the natural wake (see center and bottom images in Fig. 3), producing a jet rather than a wakelike mean-velocity profile downstream of the airfoil (as confirmed from mean-velocity measurements across the wake, shown to the right of the images in Fig. 3).

The above physical picture forms the foundation of the wake model studied here. In particular, we attempt to predict the velocity field of the wake from the superposition of an array of finite-core vortices onto a uniform flow representing the freestream. Fundamentally, our model is similar in nature to the classical Kármán vortex street model [14] with the important exception that the latter is based on inviscid point vortices. Finite-core models are, of course, in common use in "vortex blob" computational methods, which is reviewed in detail by Leonard [15]. In our model, the viscous core is accounted for using Gaussian vorticity variation of the form:

$$\omega(r) = \omega_{\max} e^{-(r/R)^2} \quad (1)$$

where  $\omega_{\max}$  is the vorticity at the vortex center,  $r$  is the radial coordinate measured from the vortex center, and  $R$  is the vortex core radius. The corresponding circulation profile is given by:

$$\Gamma(r) = \Gamma_o [1 - e^{-(r/R)^2}] \quad (2)$$

where  $\Gamma_o$  is the vortex circulation in the limit  $r \rightarrow \infty$ . It can be shown that the streamwise and transverse components of the induced velocity resulting from the superposition of  $N$  vortices and a uniform flow are given by:

$$u(x, y) = U_\infty - \sum_{i=1}^N \frac{\Gamma_i(r_i)}{2\pi} \frac{(y - y_{ci})}{r_i^2} \quad (3)$$

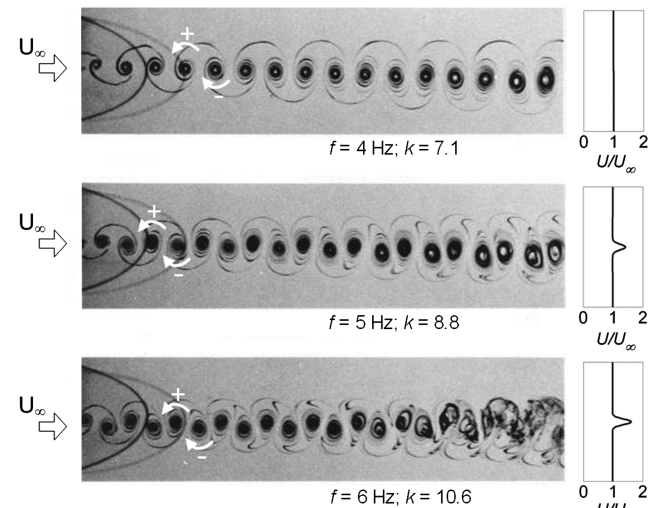
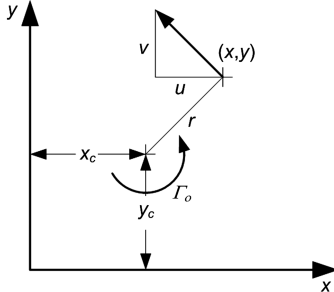


Fig. 3 Dye flow visualization images from Koochesfahani [10] depicting the wake behind the airfoil when oscillating harmonically at different frequencies. The measured streamwise mean-velocity profile associated with each case is displayed on the right of the image. White arrows indicate the sense of circulation of a counter-rotating vortex pair shed in one cycle.



**Fig. 4** Sketch illustrating different variables associated with the vortex model. The vector at  $(x, y)$  is the velocity induced by a single vortex with center at a distance  $r$  away, at  $(x_c, y_c)$ .

$$v(x, y) = \sum_{i=1}^N \frac{\Gamma_i(r_i)}{2\pi} \frac{(x - x_{ci})}{r_i^2} \quad (4)$$

where  $x_{ci}$  and  $y_{ci}$  are the streamwise and transverse coordinates, respectively, of the  $i$ th vortex center (also location of maximum vorticity). Figure 4 illustrates the induced velocity at point  $(x, y)$  caused by the presence of a single vortex at  $(x_c, y_c)$ . The figure also provides definitions of the various variables and parameters of the vortex array model.

The vortex array configuration relevant to the pure-harmonic oscillation case is depicted in Fig. 5 where two line arrays of counter-rotating vortices are symmetrically placed above and below the wake's centerline. Referring to the figure, the vortex spacing is denoted by  $a$  in the streamwise direction (this is also the oscillation wavelength) and  $b$  along the transverse direction. Equations (3) and (4) are used to calculate the induced velocity at  $x_m$  for the time instant corresponding to the vortex center locations shown in Fig. 5. This initial condition is somewhat arbitrary, but results are independent of the starting phase of the calculation (e.g., if the negative vortex is located at  $x_m$  at  $t = 0$ ). The calculation is then advanced in time over an increment  $\Delta t$  by displacing the vortex cores a distance  $U_c \times \Delta t$  (where  $U_c$  is the convection velocity) in the positive  $x$  direction and the corresponding velocity field is computed. The process is repeated over as many time increments as necessary to span one oscillation period. Note that  $U_c$  is taken as the streamwise velocity induced at the center of the vortex located at  $x_m$  at  $t = 0$  (see Fig. 5). Also, any evolution of the vortex pattern with downstream distance due to mutual interaction of the vortices is neglected; i.e., as it travels downstream, the vortex pattern arrangement is frozen. This simplification is justified by evidence obtained from the flow visualization depicted in Fig. 3, showing a stable vortex pattern over many wavelengths.

It should be evident that the model requires specification of several parameters:  $\Gamma_o$ ,  $R$ ,  $a$ ,  $b$  (note  $y_c = \pm b/2$ ), and  $N$ ; or equivalently the streamwise length spanned by the vortex array:  $L_x = (N/2 - 1)a$ . For all data presented here,  $L_x/a$  is always set to an even number with a minimum value of 2. ( $N = 6$ ). The values for all parameters are

initially set by visually matching the model prediction to the LDV measurements of  $u$  at selected phases of the oscillation cycle (except for  $N$ , which is set based on the convergence of the summations in Eqs. (3) and (4); and the wavelength, which is a dependent parameter given by  $a = U_c/f$ ). Subsequently, these “rough” initial parameter values are used to initialize a steepest-descent optimization routine that identifies the parameter values that minimize the mean squared error between the model prediction and LDV measurements of the root mean square (rms) streamwise velocity profile  $u_{rms}$  across the wake. The selection of  $u_{rms}$  instead of the mean velocity  $U$  as the quantity to minimize is because the former is found to exhibit higher sensitivity to change in model parameters. Furthermore, in comparison to optimization of the parameters based on the instantaneous velocity at a few selected phases,  $u_{rms}$  contains information from all phases of oscillation. Hence, the use of  $u_{rms}$  avoids biasing the model parameters selection to a few oscillation phases at the expense of others.

For all calculations reported here, the velocity is computed over the range  $y/C = -0.5$  to  $0.5$  at 100 different time steps per oscillation cycle (i.e., 100 phases per period). The number of positive or negative vortices is always kept odd; and the  $x$  location of the computation ( $x_m$ ) is taken as that of the center of the middle positive vortex at  $t = 0$  (marked by the broken line in Fig. 5).

Figure 6 shows the model predictions of the transverse profiles of the mean streamwise velocity  $U$ , the rms of the streamwise velocity fluctuation  $u_{rms}$ , and transverse velocity fluctuation  $v_{rms}$  for different streamwise vortex array lengths:  $L_x/a = 2, 4$ , and  $32$  ( $N = 6, 10, 66$ ). The case considered in the figure is that of harmonic oscillation at  $k = 10.6$  since this is the case that is found to be most sensitive to the number of vortices included in the model. As seen in the figure, for  $L_x/a \geq 4$ , it is difficult to discern any difference between the profiles. Thus, the model requires a small number of vortices to converge. However, as will be seen later, the number of vortices (or the domain size  $L_x$ ) needs to be larger when computing the drag force.

## IV. Results

### A. Pure-Harmonic Oscillation: Velocity Profiles

Figure 7 displays the computed streamwise velocity profiles at five different phases of the oscillation cycle:  $\Phi = 0, 0.12, 0.25, 0.37$ , and  $0.5$ . The phase-averaged velocity  $\langle u \rangle$  at the same phases is also calculated from the experimental data and displayed in the figure using open circles. Note that  $\Phi$  is the oscillation cycle phase in radians normalized by  $2\pi$ ; i.e.,  $\Phi$  changes from zero to one over one full cycle. Also, the vortex locations relative to the computation position ( $x_m$ ) at  $\Phi$  values of  $0, 0.25$ , and  $0.5$  are illustrated schematically beneath the velocity profiles.  $\Phi = 0$  and  $0.5$  represent the instants at which a positive and negative vortex, respectively, is located at  $x_m$ . In between, when  $\Phi = 0.25$ ,  $x_m$  is exactly in the middle between a positive downstream vortex and a negative upstream one. The optimum model parameters for the results shown in Fig. 7 are given in the caption.

Overall, the results in Fig. 7 show that the model predictions agree very well with the experimental data at different phases of the

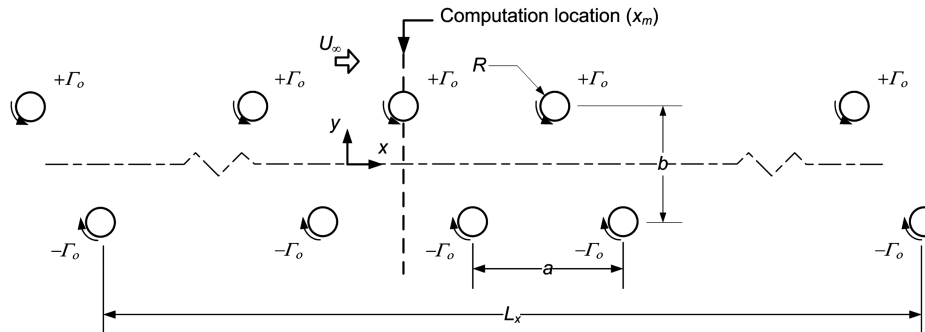


**Fig. 5** Vortex-array configuration at  $t = 0$  for modeling the wake of the airfoil undergoing pure-harmonic pitch oscillation. The location of the computation  $x_m$  is at the middle of the positive-vortex array at the instant shown.

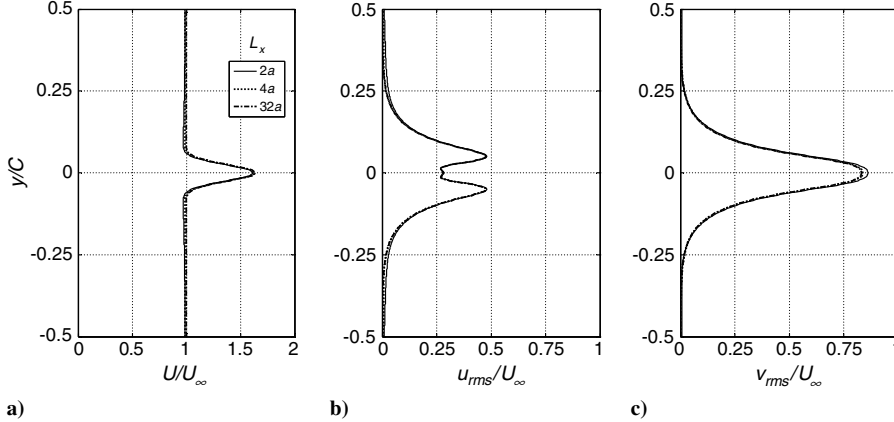


Fig. 6 Convergence of the computed velocity profiles: a) mean streamwise velocity; b) rms streamwise velocity; c) rms transverse velocity. Legend depicts values of  $L_x$ .

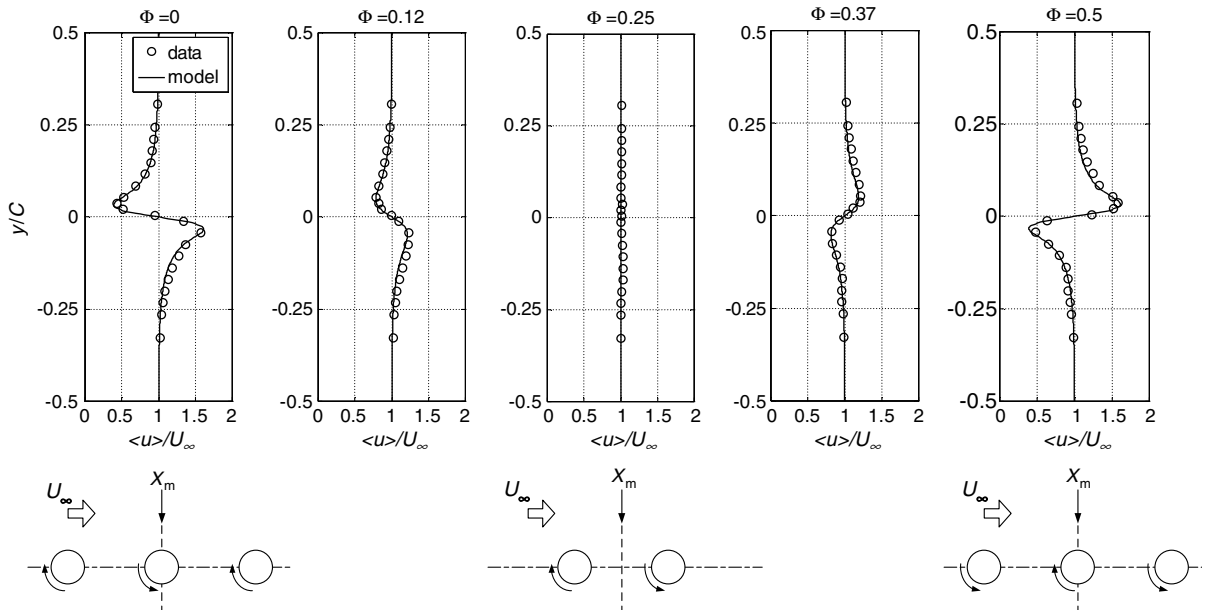


Fig. 7 Streamwise velocity profiles at selected phases of the oscillation cycle for  $k = 7.1$ . Model parameters for profiles shown are:  $\Gamma_o/U_\infty C = 0.19$ ;  $R/C = 0.03$ ;  $a/C = 0.47$ ;  $b/C = 0$ ;  $L_x/a = 4$ . Sketches beneath plots for  $\Phi = 0, 0.25$ , and  $0.5$  display the corresponding location of the vortices relative to the streamwise location of the calculation.

oscillation cycle. Some subtle differences can be discerned. At  $\Phi = 0$  and  $0.12$ , when the positive vortex has a more dominant influence on the observed velocity, the model captures the decay of the velocity with increasing distance from the wake's centerline better for positive than for negative  $y$  values. The opposite situation is observed at  $\Phi = 0.37$  and  $0.5$ , when the negative vortex is in closer proximity to the streamwise location of the calculation. In both cases, the differences are such that the computed velocity decays slightly faster than the measured velocity as  $|y| \rightarrow \infty$ .

The computed streamwise velocity at all phases of oscillation is used to calculate the mean and rms velocity profiles across the wake. These are depicted in Fig. 8 where they are compared with their experimental counterpart. In addition, Fig. 8 contains the  $v_{rms}$  profile, which is not available from the experiment but can be calculated from the vortex array model. Both the experimental and model results show that the mean velocity in the wake is uniform and equal to the freestream velocity. The  $u_{rms}$  profile contains two peaks, one on either side of the wake's centerline, while  $v_{rms}$  exhibits a single peak on the centerline. In both cases, the peak location is consistent with the expected position of maximum induced  $u$  and  $v$  resulting from the periodic passage of vortices with their centers aligned with the wake's centerline.

The same  $u_{rms}$  profile shape is captured in both the experimental and model results, though the computed  $u_{rms}$  decays somewhat faster with increasing distance from the centerline (as also noted above in the discussion of the phase-averaged results). Aside, from this slight difference, the time-averaged statistics of  $u$  are captured quite well by the model.

The comparison between the experimental and computed data for the case of  $f = 6$  Hz ( $k = 10.6$ ) is illustrated in Figs. 9 and 10. Results for  $f = 5$  Hz are similar to those shown in the latter figures, and hence are not included in the paper. Generally, a good agreement between the model and experimental results is found in Figs. 9 and 10. For the most part, the agreement is as good as that seen earlier for  $k = 7.1$ . A couple of features that are different from the  $k = 7.1$  case are: 1) the establishment of a jetlike mean velocity profile; and 2) the observation of a third local peak in the  $u_{rms}$  profile on the wake's centerline (Fig. 10). Both of these features are captured by the model. Remarkably, the model prediction is good not only for the mean and rms but also for the phase-averaged ("instantaneous") results. It is also interesting that at this very high  $k$  value, the velocity fluctuation caused by the vortex passage is so strong that the instantaneous velocity excursion from the freestream velocity could exceed  $U_\infty$  (see  $\Phi = 0$  and  $0.5$  in Fig. 9).

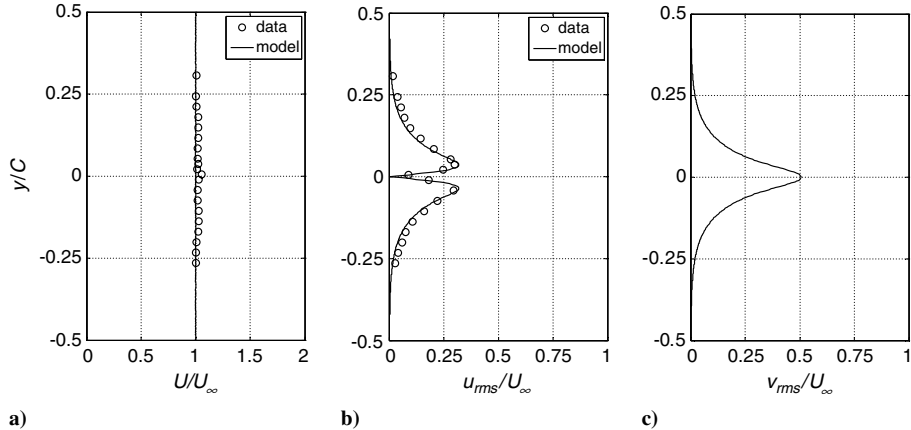


Fig. 8 Velocity profiles for  $k = 7.1$ : a) mean streamwise velocity; b) rms streamwise velocity; c) rms transverse velocity. Model parameters are given in caption of Fig. 7.

### B. Pure-Harmonic Oscillation: Comparison with Vortex Parameters Determined from Whole-Field Data

A particularly useful aspect of the present model is that it enables the use of *single-velocity-component* measurements to obtain the characteristics of the wake vortices. This is done in the present study, and the results are compared with those obtained directly from whole-field measurements by Bohl and Koochesfahani [13] in a similar experiment. The results in the latter investigation are obtained at  $x/C = 0.5$  for a NACA 0012 airfoil oscillating harmonically with pitch amplitude of  $2^\circ$  at a chord Reynolds number of 12,600. The airfoil's chord length is 12 cm and the freestream velocity is approximately 10.5 cm/s. It should be noted that although the nondimensional location at which the model results are obtained ( $x/C = 1$ ) is different from that of Bohl and Koochesfahani [13], the vortex parameters compared here change very little, if at all, between  $x/C = 0.5$  and 1 (see Bohl and Koochesfahani [13] for details).

Figure 11 displays the dependence of  $\Gamma_o$ ,  $R$ ,  $a$ , and  $b$  on the reduced frequency as obtained from the vortex array model in conjunction with the LDV data, compared with those obtained from the whole-field data of Bohl and Koochesfahani [13]. The model results are seen to be in good qualitative agreement with the experimental data. More specifically, the functional dependence of the vortex parameters on  $k$  obtained using the model is consistent with that arrived at directly from the experiment of Bohl and

Koochesfahani. Quantitatively, there is some discrepancy between the model and experimental results (except for the wavelength where a very good agreement is found).

To examine if the observed discrepancy is caused by the model or related to subtle differences in the flow studied by the Koochesfahani [10] versus that of Bohl and Koochesfahani [13], the model was used to obtain the vortex parameters for one of the cases investigated by the latter authors. The model-determined parameters agreed very well with those obtained directly from experimental data, showing that the discrepancy seen in Fig. 11 is not caused by a limitation of the vortex array model. At present the specific physical cause leading to the lack of collapse of data from the two studies is not understood.

### C. Pure-Harmonic Oscillation: Mean Streamwise Force

The mean streamwise force acting on the airfoil can be computed using the integral momentum equation. For the case of two-dimensional flow over the airfoil, the procedure yields (e.g., see Bohl and Koochesfahani [13]):

$$C_f = \frac{2}{C} \int_{-\infty}^{\infty} \left[ \frac{U}{U_\infty} \left( \frac{U}{U_\infty} - 1 \right) + \frac{u_{rms}^2}{U_\infty^2} - \frac{v_{rms}^2}{U_\infty^2} \right] dy \quad (5)$$

where  $C_f$  is the mean force coefficient (i.e., force normalized by the freestream's dynamic head, chord length, and unit span). The  $C_f$

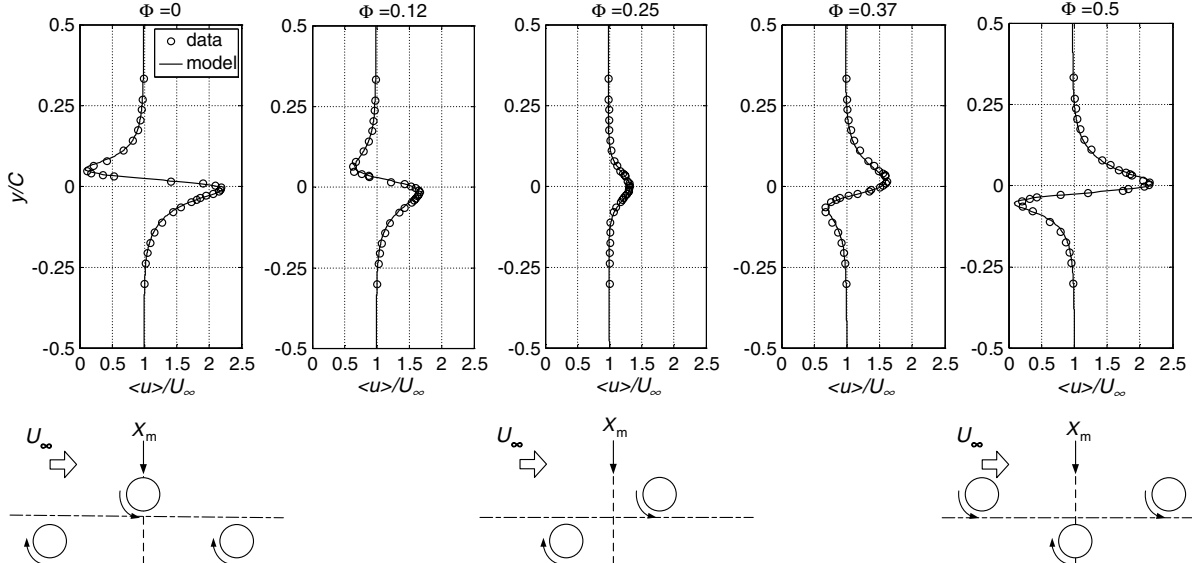
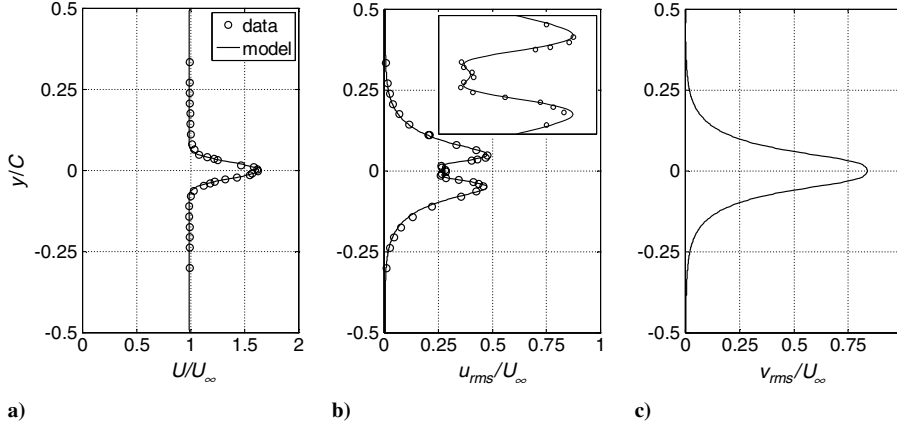


Fig. 9 Streamwise velocity profiles at selected phases of the oscillation cycle for  $k = 10.6$ . Model parameters for profiles shown are:  $\Gamma_o/U_\infty C = 0.32$ ;  $R/C = 0.029$ ;  $a/C = 0.36$ ;  $b/C = 0.045$ ;  $L_x/a = 4$ . Sketches beneath plots for  $\Phi = 0, 0.25$ , and 0.5 display the corresponding location of the vortices relative to the streamwise location of the calculation.



**Fig. 10** Velocity profiles for  $k = 10.6$ : a) mean streamwise velocity; b) rms streamwise velocity (inset shows a close-up view of the profile near  $y/C = 0$ ); c) rms transverse velocity. Model parameters are given in caption of Fig. 9.

value computed with Eq. (5) is positive when there is a net thrust acting on the airfoil and negative for a net drag. It is also notable that there are two terms in Eq. (5) that relate to the time-dependent component of the velocity, namely  $u_{rms}$  and  $v_{rms}$ . Although these terms may be ignored when analyzing the natural wake (where the fluctuating velocity may be a small fraction of the mean velocity), they must be included in the present analysis (where the instantaneous velocity can be as large as, or even greater than  $U_\infty$ ; e.g., see  $\Phi = 0$  in Fig. 9, and the peak rms velocity values are of order  $U_\infty$ , see Fig. 10). Also, it is instructive to point out that the  $v_{rms}$  term in Eq. (5) accounts for the mean-pressure variation across the wake.

In practice, Eq. (5) needs to be integrated over a large enough  $y$  range to ensure that  $U$  has converged to  $U_\infty$ . In experiments, the extent of the  $y$  domain is typically limited by the measurement range and certain corrections need to be applied. Although, in principle, a similar limitation does not exist when using the vortex array model to obtain the velocity profiles,  $U$  approaches  $U_\infty$  very slowly with increasing  $|y|$ , and hence the mean velocity may not be within an acceptably small tolerance around the freestream value at the edge of the integration domain. Therefore, in computing  $C_f$ , we employ the same expression used by Bohl and Koochesfahani [13], which takes into account the effect of truncating the integration domain:

$$C_f = \frac{2}{C} \int_{-H}^H \left[ \frac{U}{U_\infty} \left( \frac{U}{U_\infty} - 1 \right) + \varepsilon \left( \frac{U}{U_\infty} - 1 \right) + \frac{v_{rms}^2}{U_\infty^2} + \frac{1}{2} \left( 1 - \frac{U_o^2}{U_\infty^2} \right) \right] dy \quad (6)$$

where  $U_o$  is the mean streamwise velocity at the top or bottom extents of the integration domain ( $y = \pm H$ ), and  $\varepsilon$  is given by:

$$\varepsilon = \frac{1}{2} \left( 1 - \frac{U_o}{U_\infty} \right) \quad (7)$$

Using Eq. (6),  $C_f$  is computed for the case of  $k = 10.6$  using different values of  $L_x$ . The results are displayed in Fig. 12 for different control-volume widths ( $2H$ : indicated by the legend in the figure). As seen from the left plot in Fig. 12, where  $L_x$  is normalized by the wavelength  $a$ , the vortex array length required for the  $C_f$  value to converge (i.e., become independent of  $L_x$ ) is sensitive to  $2H$ : the wider the control volume, more wavelengths (i.e., the larger the number of vortices) must be maintained in the model for convergence of  $C_f$ . The results also suggest that  $L_x$  of more than approximately  $8a$

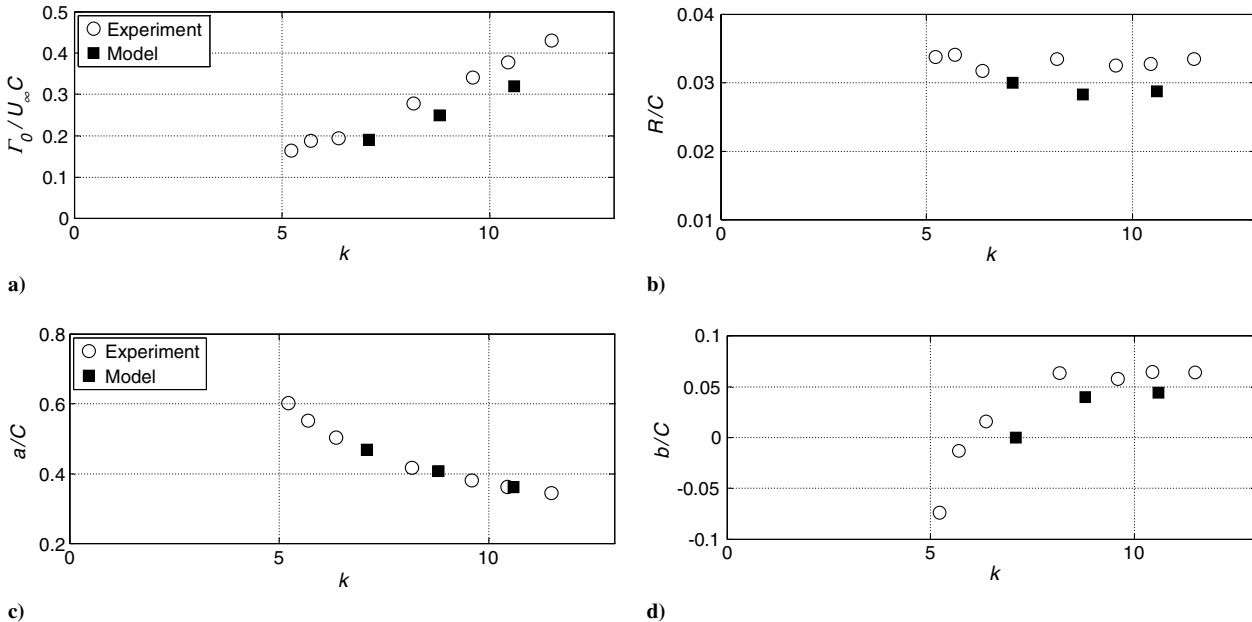


**Fig. 11** Comparison between the wake vortex parameters determined experimentally (open symbols) by Bohl and Koochesfahani [13] and those obtained here using the vortex array model: a) circulation; b) core radius; c) wavelength; d) transverse vortex spacing.

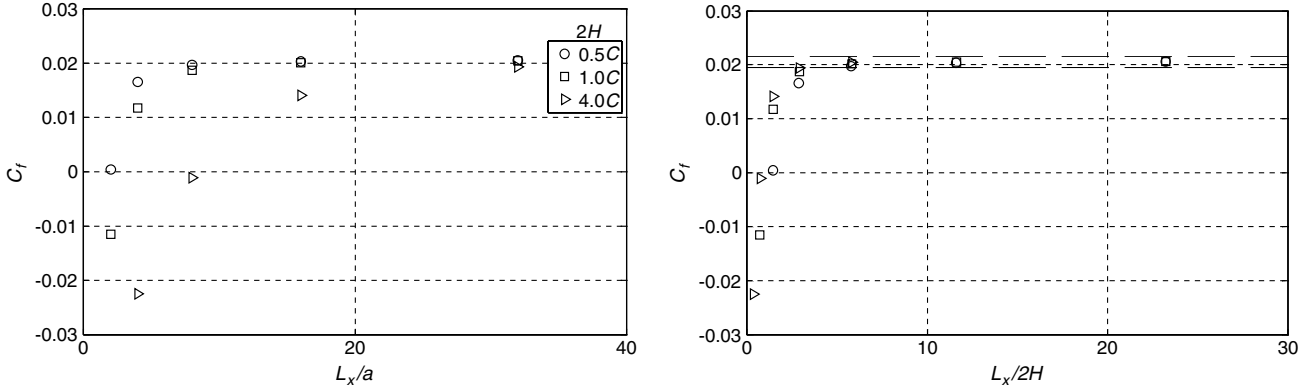


Fig. 12 Dependence of the computed  $C_f$  value on the length of the vortex array normalized by wavelength (left) and transverse control volume width (right). Legend indicates the transverse width of the control volume and broken lines outline  $\pm 5\%$  of the  $C_f$  value after convergence.

is required for the convergence, which is larger than found earlier for the velocity results.

The dependence of the convergence results on the control volume width can be eliminated by normalizing  $L_x$  by the latter, as done in the right plot in Fig. 12. Inspection of this plot suggests that a vortex array length of more than 5 times the control-volume width is required for  $C_f$  to converge to within  $\pm 5\%$  (this tolerance band is indicated by the broken lines in the plot).

The computed  $C_f$  values are compared with those obtained from the experiments of Koochesfahani [10], Bohl [12], and Bohl and Koochesfahani [13] as well as the computation of Ramamurti and Sandberg [16] in Fig. 13. Two sets of results are depicted: one based on the mean-velocity profile only ( $C_{f,mean}$ ), and the other accounting for all terms in Eq. (6). Figure 13 shows that the  $C_f$  values obtained from the vortex array model are consistent with both experiments and computations. Also the figure shows that ignoring the fluctuating-velocity terms in Eq. (6) produces large errors, including underprediction of the  $k$  value at which the net force acting on the airfoil switches from drag to thrust (corresponding to change of the sign of  $C_f$  from negative to positive). This observation was noted by Ramamurti and Sandberg [16] in their computation of the cases investigated by Koochesfahani [10]. A similar conclusion, regarding the overestimation of thrust using only mean-velocity wake surveys, was made earlier by Streitlien and Triantafyllou [17] using numerical simulation of a flapping airfoil.

Streitlien and Triantafyllou [17] also employed the von Kármán vortex street model to compute the streamwise force acting on the airfoil. They found the model to lead to surprisingly good prediction of the thrust force; though the discrepancy between the model and numerical predictions became larger with increasing reduced frequency, reaching its largest value at the highest reduced frequency investigated (a value of 2 based on their definition of the reduced

frequency; equivalent to  $k = 1$  in the present study). The success of the present model in estimating the force coefficient up to an order of magnitude larger reduced frequency is likely the result of the more realistic representation of the wake vortices by employing a viscous core.

#### D. Nonharmonic Oscillation: Velocity Profiles

The flow visualization of Koochesfahani [10] (reproduced in Fig. 14) reveals that altering the waveform of the airfoil pitch oscillation significantly changes the wake structure. For the case of  $S = 38\%$  (see Fig. 2 and Sec II for definition), a single positive vortex is produced during the shorter pitch-up period, while two negative vortices form during the longer pitch-down phase. To model this scenario, three vortex structures must be accounted for per oscillation cycle (rather than two as done in the pure-harmonic cases earlier).

A sketch of the vortex configuration used to model the  $S = 38\%$  case is shown in Fig. 15, along with the relevant parameter values. It is interesting to note that, unlike the pure-harmonic case where the vortex pattern remains practically invariant with downstream distance, Fig. 14 shows that the pattern clearly evolves in the case of nonharmonic oscillations. This implies that each of the three vortex structures shed per cycle has a different convection velocity. In obtaining the model predictions  $U_c$  is set to the average convection velocity of all three structures:  $U_c = 1.02U_\infty$ . Interestingly, this value is the same as that of the positive vortex (numbered vortex 1 in the sketch in Fig. 15). Moreover, it is found that the model predictions arrived at using this  $U_c$  value agreed with the experimental results better than when using the convection velocity of either of the negative vortices ( $0.9$  and  $1.13$  of  $U_\infty$  for the vortex with center located at positive and negative  $y$  value, respectively).

The phase-average results at selected phases and the mean as well as the rms profiles of the computed and measured velocity are displayed in Figs. 16 and 17, respectively. The results indicate that the model predicts the velocity field of the wake very well even when the oscillation is nonharmonic. It is particularly interesting to note the fairly “wild” variation in the  $u_{rms}$  profile in Fig. 17 and how this

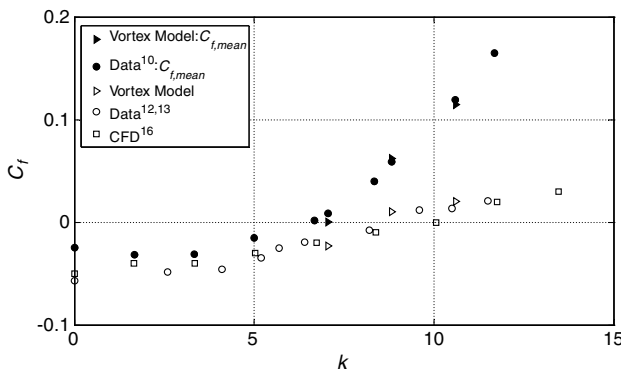


Fig. 13 Comparison of the model predictions of  $C_f$  to other experimental and numerical studies. Closed symbols give  $C_{f,mean}$ , which is the mean streamwise force coefficient calculated from the mean-velocity distribution only; open symbols represent  $C_f$  based on all integrand terms in Eq. (6).

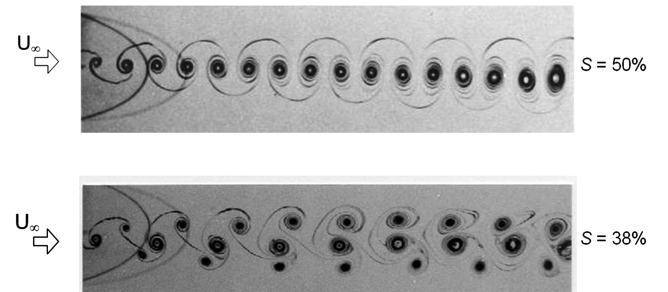


Fig. 14 Dye flow visualization images from Koochesfahani [10] depicting the wake behind the airfoil when oscillating harmonically (top) and nonharmonically (bottom).

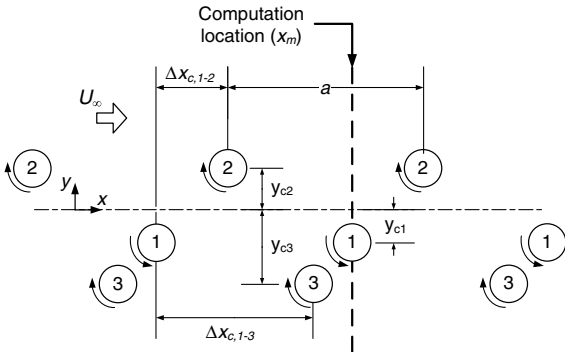


Fig. 15 Vortex-array configuration at  $t = 0$  for modeling the wake of the airfoil undergoing pitch oscillation with  $k = 7.1$  and  $S = 38\%$ . Model parameters for this case are set to:  $\Gamma_o/U_\infty C = 0.23, -0.12, -0.11; R/C = 0.0287, 0.0287, 0.0263; y_c/C = -0.066, 0.08, -0.2$  for vortices 1, 2, and 3, respectively, and  $a/C = 0.48; \Delta x_{c,1-2}/a = 0.38; \Delta x_{c,1-3}/a = 0.82$ .

variation is reproduced, practically exactly, using the vortex array model.

## V. Conclusions

The present work demonstrates that when a well-defined pattern of vortices forms in the wake of periodically pitching airfoils, the velocity in the wake can be modeled using an array of Gaussian-core vortices superimposed onto a uniform flow. This statement holds for pure-harmonic pitch oscillation, where two counter-rotating vortex structures are shed per cycle, as well as for nonpure-harmonic cases, where the vortex shedding pattern can become quite exotic. The vortex array model can be useful in determining the wake's vortex-structure characteristics from single-component velocity surveys in the wake. Moreover, if one is able to establish a rational relationship between the airfoil motion trajectory and the vorticity distribution further downstream in the wake, the model can become a useful design tool to compute the mean force acting on the airfoil.

The downstream variation of the vortex pattern in the non-harmonic case is expected to impact the model prediction due to the

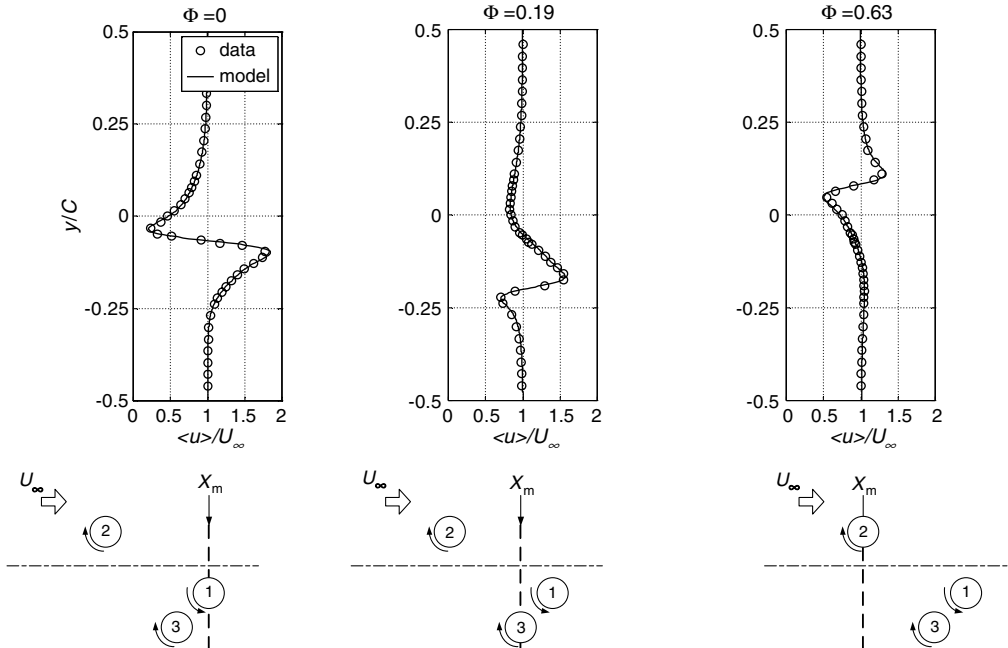


Fig. 16 Streamwise velocity profiles at selected phases of the oscillation cycle for  $k = 7.1$  and  $S = 38\%$ . Model parameters for profiles shown are as given in the caption of Fig. 15. Sketches beneath plots display the corresponding location of the vortices relative to the streamwise location of the calculation.

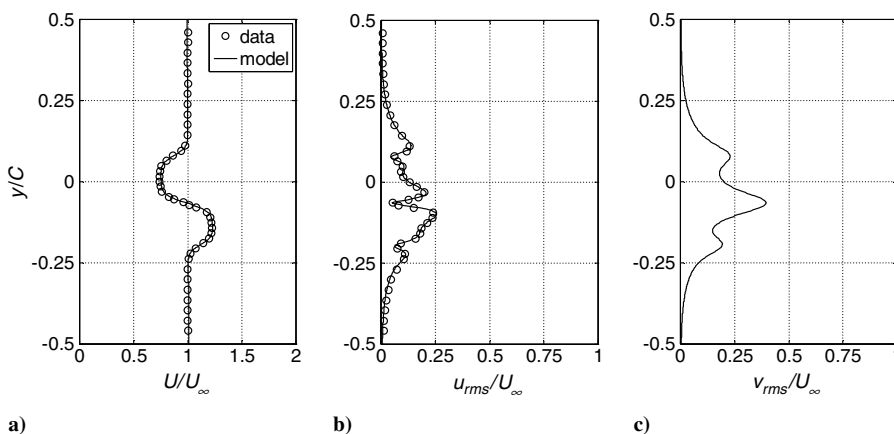


Fig. 17 Velocity profiles for  $k = 7.1$  and  $S = 38\%$ : a) mean streamwise velocity; b) rms streamwise velocity; c) rms transverse velocity. Model parameters for profiles shown are given in caption of Fig. 15.

difference between the calculated induced velocity from the assumed frozen pattern and that from the actual pattern. The difference will be related to the dipole and higher-order poles of the vortex pattern in each wavelength. The farther downstream locations have a vortex pattern that deviates more from the assumed frozen pattern at the  $X/C = 1$  location, resulting in a larger deviation in the higher-order poles of the vortex pattern, but at the same time the impact is much reduced because the induced velocity drops at least quadratically with distance. The net effect is expected to be minimal. The fact that the model prediction presented agrees so well with the measurements supports this assertion.

## References

- [1] Wilson, J. R., "Mini Technologies for Major Impact," *Aerospace America*, May 1998, pp. 36–42.
- [2] Lai, J. C. S., and Platzer, M. F., "Jet Characteristics of a Plunging Airfoil," *AIAA Journal*, Vol. 37, No. 12, 1999, pp. 1529–1537.  
doi:10.2514/2.641
- [3] Young, J., and Lai, J. C. S., "Oscillation Frequency and Amplitude Effects on the Wake of a Plunging Airfoil," *AIAA Journal*, Vol. 42, No. 10, 2004, pp. 2042–2052.  
doi:10.2514/1.5070
- [4] Anderson, J. M., Streitlien, K., Barrett, D. S., and Triantafyllou, M. S., "Oscillating Foils of High Propulsive Efficiency," *Journal of Fluid Mechanics*, Vol. 360, 1998, pp. 41–72.  
doi:10.1017/S0022112097008392
- [5] OI, M., "Vortical Structures in High Frequency Pitch and Plunge Low Reynolds Number," AIAA Paper No. 2007-4233, 2007.
- [6] OI, M. V., Dong, H., and Webb, C., "Motion Kinematics vs Angle of Attack Effects in Hi-Frequency Airfoil Pitch/Plunge," AIAA Paper No. 2008-3822, 2008.
- [7] Theodorsen, T., "General Theory of Aerodynamic Instability and the Mechanism of Flutter," NACA TR 496, 1935.
- [8] von Kármán, T., and Sears, W. R., "Airfoil Theory for Non-Uniform Motion," *Journal of the Aeronautical Sciences*, Vol. 5, No. 10, 1938, pp. 379–390.
- [9] Shyy, W., Lian, Y., Tang, J., Liu, H., Trizila, P., Stanford, B., Bernal, L., Cesnik, C., Friedmann, P., and Ifju, P., "Computational Aerodynamics of Low Reynolds Number Plunging, Pitching and Flexible Wings for MAV Applications," AIAA Paper No. 2008-523, 2008.
- [10] Koochesfahani, M. M., "Vortical Patterns in the Wake of an Oscillating Airfoil," *AIAA Journal*, Vol. 27, No. 9, 1989, pp. 1200–1205.  
doi:10.2514/3.10246
- [11] Cimbala, J. M., Nagib, H. M., and Roshko, A., "Large Structure in the Far Wakes of Two-Dimensional Bluff Bodies," *Journal of Fluid Mechanics*, Vol. 190, 1988, pp. 265–298.  
doi:10.1017/S0022112088001314
- [12] Bohl, D. G., "Experimental Study of the 2-D and 3-D Structure of a Concentrated Line Vortex," Ph.D. Thesis, Michigan State Univ., 2002.
- [13] Bohl, D. G., and Koochesfahani, M. M., "MTV Measurements of the Vertical Field in the Wake of an Airfoil Oscillating at High Reduced Frequency," *Journal of Fluid Mechanics*, Vol. 620, 2009, pp. 63–88.  
doi:10.1017/S0022112008004734
- [14] von Kármán, T., and Burgess, J. M., "General Aerodynamic Theory: Perfect Fluids," *Aerodynamic Theory*, edited by W. F. Durand, Vol. II, Springer, Berlin, 1934.
- [15] Leonard, A., "Vortex Methods for Flow Simulation," *Journal of Computational Physics*, Vol. 37, No. 3, 1980, pp. 289–335.  
doi:10.1016/0021-9991(80)90040-6
- [16] Ramamurti, R., and Sandberg, W., "Simulation of Flow About Flapping Airfoils Using Finite Element Incompressible Flow Solver," *AIAA Journal*, Vol. 39, No. 2, 2001, pp. 253–260.  
doi:10.2514/2.1320
- [17] Streitlien, K., and Triantafyllou, G. S., "On Thrust Estimates for Flapping Foils," *Journal of Fluids and Structures*, Vol. 12, No. 1, 1998, pp. 47–55.  
doi:10.1006/jfls.1997.0123

M. Visbal  
Associate Editor